ELSEVIER

Chemical Engineering Journal 77 (2000) 137–142

Chemical Engineering Journal

www.elsevier.com/locate/cej

Optical tomography for dielectric profiling in processing electronic materials

L. Zeni *, R. Bernini, R. Pierri

Dipartimento di Ingegneria dell'Informazione, Seconda Università di Napoli, Via Roma 29, I-81031 Aversa, Italy

Abstract

Optical methods represent a powerful tool for contactless characterisation of materials in industrial processes. In particular, in the microelectronic field great impetus has been given to the on-line measurement of the doping profiles in large scale productions in order to increase the overall equipment effectiveness. In this framework, we propose a new technique based on optical tomography able to reconstruct the doping profiles in semiconductor wafers starting from reflected intensity measurements, taken at infrared wavelengths. Several numerical simulations have shown the effectiveness of the proposed approach. In particular, the reconstruction of typical shallow doping profiles, generated by a process simulator, has been performed with relatively high accuracy. ©2000 Elsevier Science S.A. All rights reserved.

Keywords: Optical tomography; Doping profile; Semiconductor material; Contactless measurements

1. Introduction

In the last years a great effort has been devoted to the development of new materials and process characterisation techniques [1]. In fact, the measurement of material characteristics provides both a check on the fabrication processes [2] and a tool to improve the reliability of process simulators as well. In particular, in microelectronics (semiconductor materials and devices) and optoelectronics (optical fibers and planar waveguides), where the material properties are determined by the intentional implant or diffusion of impurities, the exact control and measurements of doping profiles, or refractive index variations, is a very crucial problem [3]. Hence, many different methods have been developed to this purpose. However, the most widely used, mainly in semiconductor industries, require the destruction of the sample under test or the realisation of suitable test structures which can change the doping profile to be measured. On the other hand, completely contactless optical techniques have been recently developed, but they only permit to reconstruct doping profiles representable by well known analytical functions [4,5].

In this work we propose a new non-destructive and contactless method for the characterisation of one-dimensional doping profiles in semiconductor wafers. Our approach relies on optical diffraction tomography, where the complex permittivity of a weakly scattering inhomogeneous object, illuminated by a known wavefield at different wavelengths and/or different directions, is reconstructed starting from the measurements of reflected and/or transmitted field.

The proposed technique, starting from infrared spectroscopy data, allows to reconstruct one-dimensional profiles in semiconductor samples, and could be used for both ex situ and in situ monitoring of technological process [2]. In our approach, we assume that only the field intensity is available. Using the integral relations of the electromagnetic scattering [6], under a linear approximation, and taking advantage of the linear relationship, which holds true at infrared wavelengths, between the free carriers concentration and the complex permittivity of the semiconductor material, we relate the field intensity reflected by the sample to the doping profile [7]. The reconstruction problem is formulated as the minimisation of a proper non-linear functional representing the error between the measurements of the reflected intensity, at different frequencies, and the model data. In our approach the unknown carriers concentration profile is not described by a 'parametric' expression of a known function [4], but an expansion in a finite series of basis functions is used. So, no 'strong' assumption must be made on the functional form of the doping profile (e.g. exponential function, Gaussian function, error function, etc.). Furthermore, this particular choice of the data and unknowns allows us to tackle a quadratic inverse problem that has already been faced in the literature addressing and solving the problem of the presence of local minima,

* Corresponding author. Tel.: +39-81-5010269; fax: +39-81-5037042.
E-mail address: zeni@unina.it (L. Zeni).

1385-8947/00/$ – see front matter ©2000 Elsevier Science S.A. All rights reserved.
PII: S1385-8947(99)00141-2

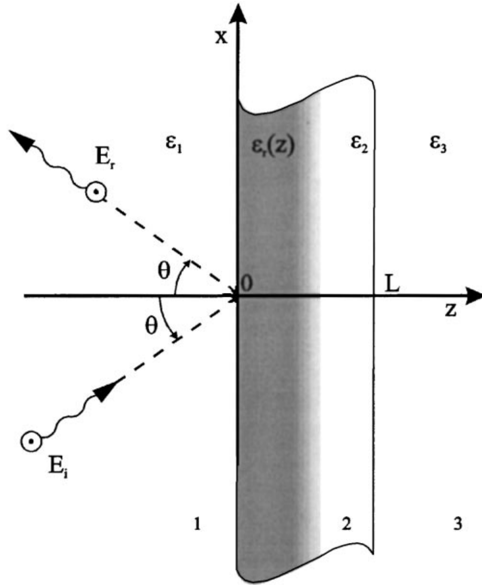

Fig. 1. The geometry of the problem.

typical of any non-linear inversion [8]. The effectiveness of this approach is demonstrated by numerically simulating the measurements.

2. Formulation of the problem

In Fig. 1 is depicted the geometry of the one-dimensional problem considered: a homogeneous slab, of thickness L, with a non-homogenous material embedded. The slab and the non-homogenous material are characterised by the constitutive parameters $\{\mu_0, \varepsilon_0\varepsilon_2\}$ and $\{\mu_0, \varepsilon_0\varepsilon_r(z)\}$, respectively, where ε_2 is the relative dielectric permittivity of the homogeneous slab and ε_r is the relative dielectric permittivity of the non-homogenous material. The constitutive parameters of the front and back medium are $\{\mu_0, \varepsilon_0\varepsilon_1\}$ and $\{\mu_0, \varepsilon_0\varepsilon_3\}$, respectively. μ_0 is the magnetic permeability of the vacuum.

The slab is illuminated by a plane wave E_i with the electric field vector perpendicular to the plane of incidence, at an angular frequency ω from a fixed angle θ. The total electric field E_r reflected by the sample is related to the dielectric permittivity $\varepsilon_r(z)$ by Helmholtz scalar wave equation [6]:

$$\frac{\partial^2 E_r}{\partial z^2} + k_z^2(z) E_r = 0 \tag{1}$$

with

$$k_z(z) = \sqrt{\varepsilon_r(z) k_0^2 - (k_1 \sin(\theta))^2} \tag{2}$$

$k_0 = \omega\sqrt{\mu_0\varepsilon_0} = 2\pi/\lambda$ being the wavenumber of the vacuum.The unknown dielectric profile $\varepsilon_r(z)$, can be expressed as the superposition of the dielectric permittivity of the homogeneous slab ε_2, and a perturbation χ, called 'contrast function', defined as:

$$\chi(z) = \begin{cases} (\varepsilon_r(z) - \varepsilon_2) & z \in [0, L] \\ 0 & z \notin [0, L] \end{cases} \tag{3}$$

The function $\chi(z)$ represents the new unknown of the problem. So, in this approach we do not search directly for the dielectric profile, but only for the variations with respect to the homogeneous one.

Adding and subtracting $k_{z2}^2 E_r$ into Eq. (1), where

$$k_{z2} = \sqrt{\varepsilon_2 k_0^2 - (k_1 \sin(\theta))^2},$$

the Helmholtz equation may be rewritten as:

$$\frac{\partial^2 E_r}{\partial z^2} + k_{z2}^2 E_r = -k_0^2(z)\chi(z) E_r \tag{4}$$

This equation permits to relate the reflected field to the perturbation $\chi(z)$, which appears as a source function on the right side of Eq. (4).

3. Basic equations

The solution E_r of Eq. (4) represent the field reflected by the slab at a fixed distance $\bar{z}$, and can be expressed as the sum of the field reflected by the homogeneous slab E_0 and the field reflected by the perturbation E_s, normally called scattered field [6]:

$$E_r(\bar{z}; \omega) = E_0(\bar{z}; \omega) + E_s(\bar{z}; \omega) \quad \bar{z} < 0 \tag{5}$$

where:

$$E_0(\bar{z}; \omega) = r(\omega) \exp(\mathrm{i} k_{z1} \bar{z}) \tag{6}$$

with [6]:

$$r(\omega) = -R_{21} + \frac{T_{12} R_{23} T_{21} \exp(-\mathrm{i}2k_{z2}L)}{1 - R_{21} R_{23} \exp(-\mathrm{i}2k_{z2}L)} \tag{7}$$

$$k_{z1} = k_1 \cos(\theta) \tag{8}$$

$k_1 = \omega\sqrt{\mu_0\varepsilon_1\varepsilon_0}$ being the wavenumber of the front medium, R_{nm}, T_{nm} the reflection and transmission coefficients between the medium n and the medium m [6], respectively (see Fig. 1).

If we assume that χ represent a weak perturbation respect to the homogeneous slab, $\chi(z) \ll \varepsilon_2$, the scattered field can be expressed as [6]:

$$E_s(\bar{z}; \omega) = k_0^2 \int_0^L G(\bar{z}, z'; \omega)\chi(z') E_{io}(z'; \omega)\, \mathrm{d}z' \tag{9}$$

$G(\bar{z}, z'; \omega)$ is the Green function for $\bar{z} < 0$, that is the solution of Eq. (4) when the source term on the right hand-side is $-\delta(\bar{z} - z')$, and is expressed by [6]:

$$G(\bar{z}, z'; \omega) = \frac{T_{21} h(z') \exp(\mathrm{i}k_{z1}\bar{z})}{\mathrm{i}2k_{z2}(1 - R_{21}R_{23}\exp(-\mathrm{i}2k_{z2}L))} \tag{10}$$

with

$$h(z') = \exp(-\mathrm{i}k_{z2}z') + R_{23}\exp(-\mathrm{i}2k_{z2}L)\exp(\mathrm{i}k_{z2}z')$$

and E_{io} is the electric field inside the homogeneous slab [6]:

$$E_{io}(z'; \omega) = \frac{T_{12} h(z')}{(1 - R_{21} R_{23} \exp(-i2k_{z2}L))} \quad (11)$$

This approximation, also called weak scattering approximation or distorted Born approximation, permits to linearly relate the scattered field to the dielectric properties of the inhomogeneous material embedded in the slab.

Starting from the knowledge of E_s at different wavelengths and/or different directions of incident field, several methods have been developed in order to invert Eq. (9) and reconstruct the function $\chi(z)$ [6,9,10].

4. Semiconductor dielectric function

For a semiconductor material the dielectric permittivity can be expressed as the sum of the lattice ε_L and free-carriers contributions ε_C:

$$\varepsilon(z; \omega) = \varepsilon_L(\omega) + \varepsilon_C(z; \omega) \quad (12)$$

The lattice contribution can be expressed as a function of radiation wavelength (in micron) according to the dispersion formula [11]:

$$\varepsilon_L(\lambda) = A + \frac{B}{\lambda^2} + \frac{C\lambda_1^2}{(\lambda^2 - \lambda_1^2)} \quad (13)$$

where, if silicon is concerned, $\lambda_1 = 1.1071\,\mu m$ while $A = 11.6858$, $B = 9.39816 \times 10^{-1}\,\mu m^2$ and $C = 8.10461 \times 10^{-3}$.

The free carriers contribution is due to the intraband transitions and, when the substrate and the doping material are of the same type, it can be represented, according to the Drude–Lorenz model [12], by:

$$\varepsilon_C(z; \omega) = \left[\frac{-\omega_P^2(z)}{\omega^2 + \omega_T^2(z)} + i \frac{\omega_P^2(z)\omega_T(z)}{\omega(\omega^2 + \omega_T^2(z))} \right] \quad (14)$$

where the plasma frequency $\omega_p(z)$ and the scattering frequency $\omega_T(z)$ of the free carriers are related to the semiconductor parameters by the following expressions [12]:

$$\omega_P^2(z) = \frac{N(z)e^2}{\varepsilon_0 m^*} \quad (15)$$

$$\omega_T(z) = \frac{e}{m^* \mu(z)} \quad (16)$$

e being the electron charge, m^* the effective mass, μ the free carrier mobility, $N(z)$ the free carrier concentration profile. Eq. (16) shows that the scattering frequency depends on the doping profile through the carrier mobility. Normally this effect is neglected (see [4,5]), however we shall take it into account by using an iterative procedure as explained in Section 5.

Substituting Eq. (15) into Eq. (14) we obtain:

$$\varepsilon_C(z; \omega) = C(z; \omega) N(z) \quad (17)$$

where:

$$C(z; \omega) = \frac{e^2}{\varepsilon_0 m^*} \left[\frac{-1}{\omega^2 + \omega_T^2(z)} + \frac{i\omega_T(z)}{\omega(\omega^2 + \omega_T^2(z))} \right] \quad (18)$$

Eq. (17) shows that the free carrier contribution ε_C is linearly related to the carrier concentration.

Taking into account Eqs. (12) and (17) we can write:

$$\varepsilon(z; \omega) = \varepsilon_L(\omega) + C(z; \omega) N(z) \quad (19)$$

Indicating with N_{sub} the doping concentration of the substrate and with ΔN the variation of the carrier concentration induced by the doping profile, we can write:

$$N(z) = N_{sub} + \Delta N(z) \quad (20)$$

Finally, the dielectric permittivity of the non-homogeneous material can be written as:

$$\varepsilon_r(z; \omega) = \varepsilon_2(z; \omega) + \chi(z; \omega) \quad (21)$$

where

$$\varepsilon_2(z; \omega) = \varepsilon_L(\omega) + C(z; \omega) N_{sub} \quad (22)$$

$$\chi(z; \omega) = C(z; \omega) \Delta N(z) \quad (23)$$

5. Reconstruction of doping profiles

The scattering field in the semiconductor case can be obtained by plugging Eq. (23) into Eq. (9):

$$E_s(\bar{z}; \omega) = k_0^2 \int_0^L G(\bar{z}, z'; \omega) C(z'; \omega) \Delta N(z') E_{io}(z'; \omega)\, dz' \quad (24)$$

This equation shows that, in the distorted Born approximation, the scattered field is linearly related to the carriers concentration. Starting from the knowledge of the reflected field, both in amplitude and in phase, we could retrieve the doping profiles using the algorithms that have been developed to reconstruct dielectric profiles [6,9,10]. However, the phase measurements, at optical wavelength, require methods that are quite complicated from an experimental point of view. In order to overcome this problem, we have developed a new method that requires only intensity (square amplitude) measurements at infrared wavelengths. These measurements can be easily performed using a FTIR spectrometer. The uniqueness of solution, in this case, can be ensured relying on the analytical properties of the total field. In fact, the addition of the reflected field E_0 to the scattered one E_s, satisfying the condition $|E_s| < |E_0|$, removes the ambiguities in the solution [13].

Finally, we have to invert the relation:

$$I(\omega) = F(\Delta N; \omega) \tag{25}$$

where

$$F(\Delta N; \omega) = \left| E_0(\bar{z}; \omega) + k_0^2 \int_0^L G(\bar{z}, z'; \omega) C(z'; \omega) \times \Delta N(z') E_{io}(z'; \omega)\, dz' \right|^2 \tag{26}$$

and I is the intensity of the total reflected field measured, at a fixed distance $\bar{z}$, at different wavelengths.

Although the uniqueness of the solution is ensured, since the measured values are noise affected, the problem is ill-posed [6]; therefore the problem of inverting Eq. (25) is, faced by looking for a generalised solution defined as the global minimum of the following non-linear functional:

$$\Phi = \sum_{i=1}^{V} \frac{(F_i(\Delta N) - I_i)^2}{I_i} \tag{27}$$

where the data are represented by the field intensity samples taken at V different wavelengths, while the unknown is the carrier concentration profile.

In order to perform the minimisation procedure the carrier concentration is expressed as the superposition of a finite number M of basis functions, defined in the region $D=[0, d]$ ($d \le L$) where significant variation of the concentration occurs:

$$\Delta N(z') = \sum_{q=0}^{M} a_q P_q \left(\frac{z' - d/2}{d/2} \right) \quad z' \in D \tag{28}$$

where P_q is the Legendre polynomial of order q. Substituting Eq. (28) into Eq. (26) we have:

$$F(\underline{a}; \omega) = \left| E_0(\omega) + \sum_{q=0}^{M} a_q \gamma_q(\omega) \right|^2 \tag{29}$$

where $\underline{a} = (a_0, a_1, \ldots, a_M)$ and

$$\gamma_q(\omega) = k_0^2 \int_0^d G(\bar{z}, z'; \omega) E_{io}(z'; \omega) C(z'; \omega) P_q \times \left(\frac{z' - d/2}{d/2} \right) dz' \tag{30}$$

Eq. (27) becomes:

$$\Phi = \sum_{i=1}^{V} \frac{(F_i(\underline{a}) - I_i)^2}{I_i} \tag{31}$$

So the problem of reconstructing the doping profile has been reduced to that of finding the coefficients $\underline{a} = (a_0, a_1, \ldots, a_M)$ that minimise the functional Φ. The minimisation of the function (31) is performed using a quasi-Newton algorithm; in particular, the Broyden–Flecher–Goldfarb–Shanno (BFGS) method has been chosen [14].

Using a base function expansion we have two definite advantages. First, we do not fix a priori the functional form of the doping profile using a model function (e.g. the classical solutions of the diffusion problems). This allows to reconstruct the actual profile, regardless of its similarity with the expected one. In fact, it has been observed that the actual doping profile not always agree to the model function [4]. Second, together with the choice of the field intensity as data, it permits to avoid the local minima problem. In fact, the use of a basis functions expansion let us to tackle with a quartic functional Φ whose behaviour, in terms of local minima, has been extensively examined and sufficient conditions, ensuring their absence, have been established [8].

As stressed in the above section, in order to take into account for the mobility dependence on the carriers concentration we use an iterative minimisation procedure. In the first step the mobility is a constant equal to the value relative to the substrate; the recovered doping profile is then used to calculate a mobility profile useful to perform the second step. The procedure is stopped when a negligible variation in the recovered profile is achieved.

6. Numerical results

In order to test the validity of the method, several reconstructions of doping profiles have been performed starting from synthetic data. The simulations have been performed referring to silicon wafers of thickness $L=300\,\mu m$ and with a specific doping profile, by calculating $V=84$ uniformly spaced values of the reflected intensity in the spectral range 330–8700 cm^{-1} ($1.15 \div 30\,\mu m$). The front and back media are supposed to be the air so $\varepsilon_1 = \varepsilon_3 = 1$, while the incident angle is $\theta = 5°$. In the reconstruction procedure the minimisation always starts from a flat profile ($\Delta N = 0$). The reliability of the reconstruction is evaluated by introducing the normalised mean square error defined by:

$$\text{err} = \frac{\| N - N_r \|}{\| N \|} \tag{32}$$

where N and N_r are the exact and the reconstructed profile, respectively.

The number M of the basic functions used in the reconstruction procedure can be 'guessed' relying on the a priori information about technological process employed to realise the profile under analysis. Anyway, in order to take into account the unavoidable differences between the expected profile and the actual one we have developed a 'step-by-step' procedure. We increase the number of the basic functions starting with a low value of M and increasing it at each step until the difference between two successive solutions is negligible.

The ability of the technique to reconstruct the doping distribution after different processes has been tested using

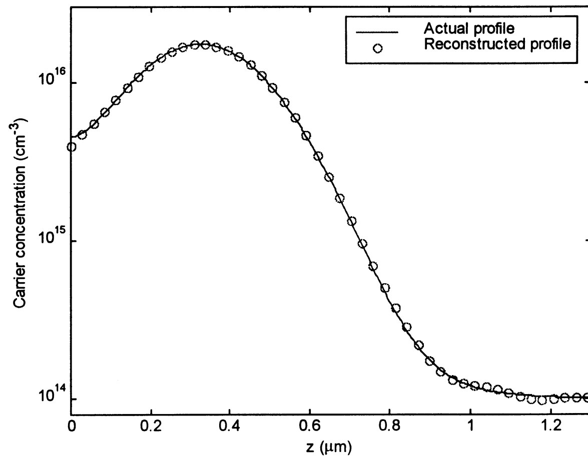

Fig. 2. Case #1: actual (solid line) and reconstructed (dotted line) profiles. The reconstruction error is 0.7%.

a one-dimensional process simulator in order to obtain the doping profiles. In particular, two cases have been considered. First, we have analysed a high-energy ion implantation followed by a short time drive-in (case #1), second a low energy ion implantation followed by a long time drive-in (case #2) has been considered. The reconstruction results are depicted in Figs. 2 and 3, respectively.

In the first case $d=1.3\,\mu$m is used while the number of basic functions has been initially fixed to $M=12$, relying on the information relative to the functional form of the profile. Then this number has been increased step-by-step up to $M=16$, when no further reduction of the reconstruction error occurs. The result of the minimisation is depicted in Fig. 2, in this case the reconstruction error is err = 0.7%.

In the second case $d=1.3\,\mu$m is used while the procedure ends with $M=11$ and err = 0.6% is achieved (see Fig. 3).

The above results clearly show the ability of our method to deal with typical doping profiles. The validity of this approach is essentially limited by the validity range of the Born approximation. In fact, it has been shown that the latter poses limitations both on the doping level and on the spatial extension of the doping profile to be reconstructed [15]. The maximum resolution achievable is related to the smallest wavelength used in the reconstruction and to the dielectric permittivity of the homogeneous slab ε_2. In particular, if $\lambda_{\min}$ is the smallest wavelength, from the analysis performed in [16], it can be estimated that the spatial resolution is about $\lambda_{\min}/(2\sqrt{\varepsilon_2})$, as it is also expected by the Rayleigh limit.

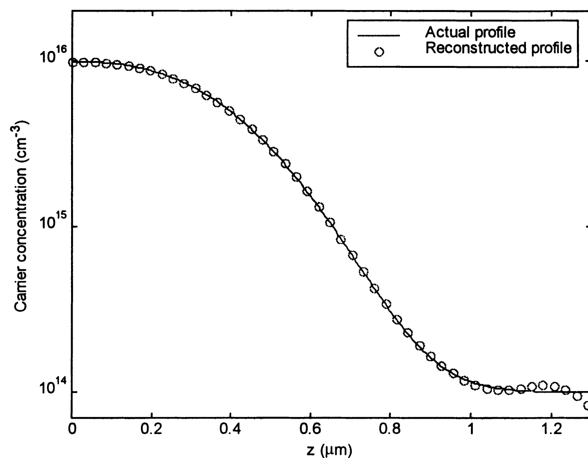

Fig. 3. Case #2: actual (solid line) and reconstructed (dotted line) profiles. The reconstruction error is 0.6%.

7. Conclusions

We have presented and numerically tested a new method useful for the non-destructive characterisation of doping profiles in semiconductor materials. This approach, differently from previous ones where phase measurements are required, needs only the measurements of the intensity reflected by the sample at different wavelengths, which can be easily performed by a FTIR spectrometer. Furthermore, the use of a basis expansion, in order to express the unknown profile, permits to avoid to choose a priori its analytical expression. The numerical simulations performed on shallow doping profiles show the good accuracy of the method.

Work is in progress to modify the present approach in order to overcome some limitations of the distorted Born approximation [17].

References

[1] M.S. Beck, T. Dyakowski, R.A. Williams, Process tomography — the state of the art, Proc. of Frontiers in Industrial Process Tomography, April 1997, Delft, The Netherlands.

[2] S. Charpenay, P. Rosenthal, G. Kneissl, C.H. Gondran, Model-based analysis for precise and accurate epitaxial silicon measurements, Solid State Technol. 41 (1998) 161–164.

[3] A.C. Diebold, M.R. Kump, J.J. Kopanski, D.G. Seiler, Characterization of the two-dimensional dopant profiles: status and review, J. Vac. Sci. Technol. B 14 (1996) 196–201.

[4] T.E. Tiwald, D.W. Thompson, J.A. Woollam, Optical determination of shallow carrier profiles using Fourier transform infrared ellipsometry, J. Vac. Sci. Technol. B 16 (1998) 312–316.

[5] H. Nakano, T. Sakamoto, K. Taniguchi, Nondestructructive measurements of thickness and carrier concentration of GaAs epitaxial layer using infrared spectroscopic ellipsometry, J. Appl. Phys. 83 (1998) 1384–1389.

[6] A.G. Tijhuis, Electromagnetic Inverse Profiling: Theory and Numerical implementation, Utrecht, VNU Science Press, 1987, pp. 108–114.

[7] L. Zeni, R. Bernini, R. Pierri, Reconstruction of doping profiles in semiconductor materials using optical tomography, Solid State Electronics 43 (1998) 761–769.

[8] R. Pierri, G. Leone, R. Bernini, Material characterization via phaseless tomography: numerical results in phase retrieval, Proc. of 1998 OSA Signal Recovery and Synthesis Topical Meeting, July 1998, Kailua-Kona, USA, pp. 130–132.

[9] G. Leone, R. Persico, R. Pierri, Inverse scattering under the distorted Born approximation for cylindrical geometries, J. Opt. Soc. Am. A 16 (1999) 1779–1787.

[10] T.C. Wedberg, J.J. Stamnes, Experimental examination of the quantitative imaging properties of optical diffraction tomography, J. Opt. Soc. Am. A 12 (1995) 493–500.
[11] E.D. Palik, Handbook of optical constants of solids, Academic Press, New York, 1985, p. 547.
[12] G. Bauer, W. Richter, Optical characterization of epitaxial semiconductor layer, Springer, Berlin, 1996, p. 203.
[13] M.H. Maleki, A.J. Devaney, Phase-retrieval and intensity-only reconstruction algorithms for optical diffraction tomography, J. Opt. Soc. Am. A 10 (1993) 1086–1092.
[14] W.H. Press, B.P. Flannery, S.A. Teukolsky, W.T. Vetterling, Numerical Recipies, Cambridge University Press, Cambridge, 1987.
[15] M. Slaney, A.C. Kak, L.E. Larsen, Limitations of imaging with first-order diffraction tomography, IEEE Trans. Microwave Theory Tech., 1984, MTT-32, pp. 860–874.
[16] R. Pierri, R. Persico, R. Bernini, Information content of the Born field scattered by an embedded slab: multifrequency, multiview, and multifrequency-multiview cases, J. Opt. Soc. Am. A, 16 (1999) 2392–2399.
[17] R. Bernini, L. Zeni, R. Pierri, An iterative method for optical reconstruction of graded index profiles in planar dielectric waveguides, Journal of Lightwave Technology, 1999, submitted for publication.